# Measurement of Reactive Mixing of Liquids with Combined PIV and Reactive PLIF Methodology

C. W. Lipp*, P. A. Gillis, R. D. Spradling, K. Tsai
Process Mixing Group
Corporate Research and Development
The Dow Chemical Company
Freeport, TX 77541-3257
[ * charlipp@dow.com ]

and

L. A. Melton
Department of Chemistry
University of Texas at Dallas
Richardson, Texas 75083-0688
[ melton@utdallas.edu ]

**ABSTRACT**

A new fluorescence-based reactive diagnostic using irreversible kinetics to test subgrid mixing Computational Fluid Dynamics (CFD) mixing models is described. The diagnostic system is based on the destruction of the fluorescent dye by Fenton's reagent, which is the combination of hydrogen peroxide and ferrous ion. The overall reaction appears to destroy the fluorphore irreversibly and to be sensitive to micromixing. A key advantage of this class of diagnostic is the spatial resolution of reaction extent, which allows a detailed comparison of experiment and CFD model.

A turbulent, Reynolds number of ca. 10,000, two-dimensional shear flow was chosen as the test case. A simultaneous PIV/PLIF methodology was chosen to maximize the information density from the experiments, but measurements are at spatial resolution far greater than the Batchelor scale (ca. 3 micrometers) for this system. Reactive diagnostics measure molecular level mixing, and thus offer advantages over dilution diagnostics. Spatial resolution of reaction extent can provide both useful engineering insight and benchmark tests of subgrid CFD models.

There is a need to develop a benchmark reacting flow geometry to allow the complexity of reacting flow modeling to be evaluated. A proposed geometry is two parallel streams entering a reacting flow region that has a backward facing step as shown below.

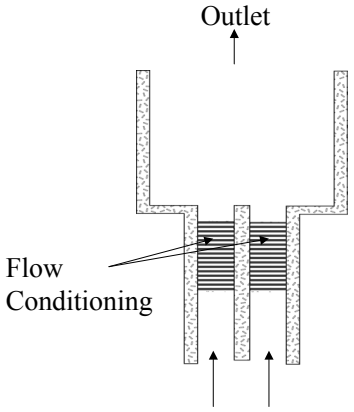


Proposed Benchmark Reacting Flow Geometry

## INTRODUCTION

Flow with chemical reaction is a commercially significant fluid dynamic system. There are many examples of reacting gas phase flow systems; these are typically combustion systems. The ability to predict selectivity and conversion is a critical measure of the ability to model any reacting flow system. Liquid phase systems are of commercial significance in the manufacturing of plastics and chemicals. Turbulent reacting flows with reaction offer a significant challenge to computational prediction. In concept several laser diagnostics can be used to select sub-grid mixing and reaction models used in RANS (Reynolds Average Navier Stokes) based CFD (Computational Fluid Dynamics). PIV (Particle Imaging Velocimetry) and PLIF (Planar Laser Induced Fluorescence) have been used to examine mixing type flows. There are many existing and proposed modeling approaches for reacting flow and the sub-grid models; however, there is a notable lack of spatially resolved data sets to evaluate different models. Komori (1993) presents an example of a data set using LIF (Laser Induced Fluorescence) to characterize a shear flow.

PLIF is used by practitioners in several ways [Catrakis and Dimotakis (1996, 1996a), Dahm and Dimotakis (1990, 1990a), Dimotakis, et al. (1983), Distelhoff, et al. (1997), Houcine, et al. (1994, 1996), Karasso and Mungal (1997), Koochesfahani and Dimotakis (1986), Miller and Dimotakis (1996), Vivier, et al. (1994), Wang and Fiedler (2000, 2000a)]. First, it can be used for qualitative flow visualization, which has minimal technical requirements for effective usage, in order to gain engineering insight. This mode is perhaps most valuable in problem-solving situations. Second, quantitative analysis of fluid mixing, such as in the analysis of a static mixer, requires more care to meet the experiment-dependent limits on uncertainties required to make sound judgments about the effectiveness of the apparatus. Third, PLIF is one of the diagnostic tools used to evaluate the applicability of subgrid mixing models used in CFD. Here, the required uncertainty must be sufficiently small to reject a model at a required confidence level, typically 95%. A detailed discussion of the statistical methods required is beyond the scope of this paper but has been presented in detail elsewhere [Coleman and Steele (1989)]. It is desirable to carry out such analysis before any experimental work begins and to reanalyze the uncertainties once the experiment is underway. In each of these cases, the actual use of PLIF should be tailored to the uncertainty required to make a judgment.

Simultaneous use of PLIF and PIV can provide substantial understanding of fluid flow and mixing phenomena [Sen, et al. (1999), Boedec and Simoens (2001), Hasselbrink (1998)]. Most commercial PIV apparatus makes use of laser sheets formed from the 532 nm second harmonic of the Nd:YAG laser, and hence, fluorophores that can be excited effectively at 532 nm are highly desirable.

Rhodamine WT (Rh-WT) [CAS Registry Number 37299-86-8; CA Index Name Xanthylium, 9-(2,4-dicarboxyphenyl)-3,6-bis(diethylamino)-chloride, disodium salt] was obtained from Turner Designs, Inc. [Turner (2001)] and was used without further purification. Rh-WT is closely related to Rhodamine B, and its spectral properties are quite similar to those of Rhodamine B. The structure of Rh-WT is shown in Figure 1, and its absorbance/fluorescence spectra are shown in Figure 2. Rh-WT absorbs strongly at 532 nm ($\varepsilon = (5.06 \pm 0.11) \times 10^4$ $M^{-1}cm^{-1}$), and fluoresces strongly ($\lambda_{max}$ = 587 nm) well away from the laser wavelength. Like Rhodamine B, its fluorescence is virtually independent of pH over the range 3-11. Rh-WT is much more soluble and reportedly much less toxic than Rhodamine B, and it is approved by the EPA for use in stream tracer studies near water supply inlets [Turner (2001)]. Its favorable spectral properties, which make simultaneous PIV/PLIF measurements feasible, and its minimal toxicity have made it our fluorophore of choice for fluid mechanics and mixing experiments.

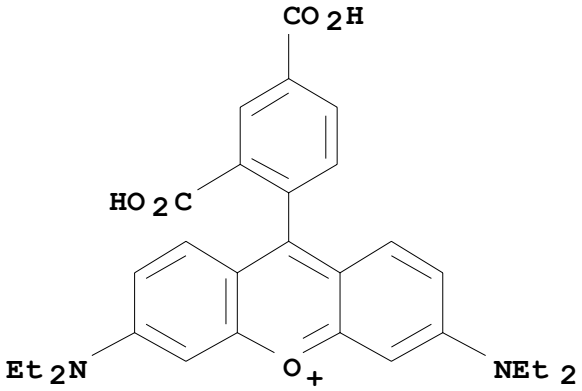


Figure 1. Chemical Structure of Rhodamine WT, a Disodium Salt

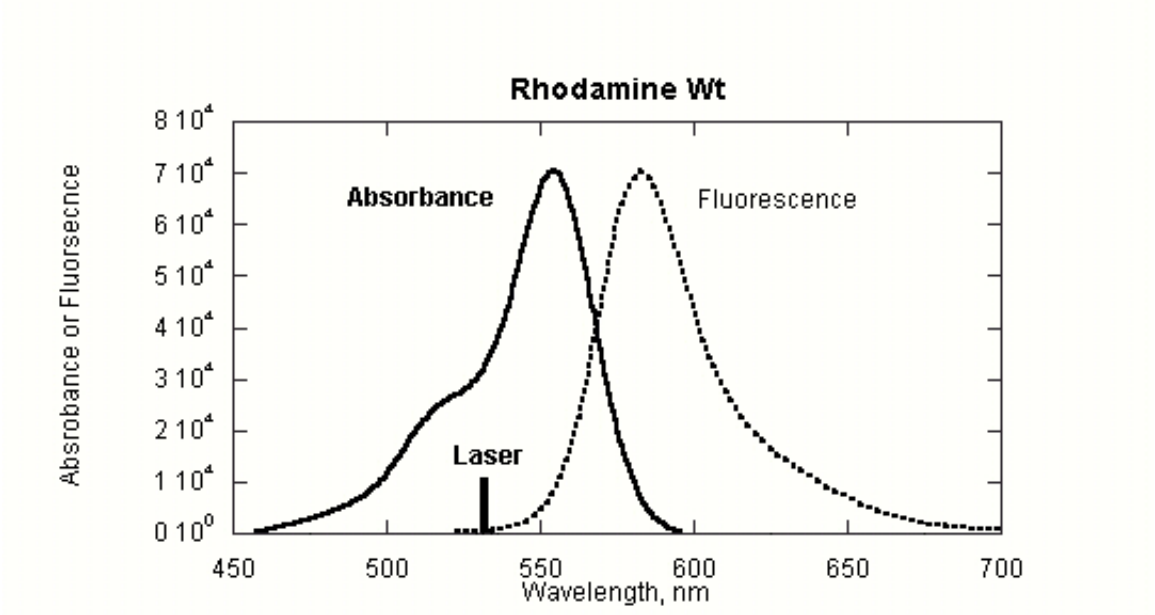


Figure 2. Spectral Response of Rhodamine WT

The reactive PLIF system that is being explored allows the measurement of reaction extent by the reduction in florescence. Both steams contain identical concentrations of Rhodamine WT. Stream A contains hydrogen peroxide and Stream B contains ferrous ammonium sulfate. Table 1 contains the summary of the reaction elementary steps and the estimated or measured reaction rates (a paper describing the reaction steps is in preparation.) Typically the concentration of Rhodamine WT used for experiments is $1.5 \times 10^{-7}$ M/liter with 0.03 M/liter hydrogen peroxide and 0.0071 M/liter ferrous ammonium sulfate. A stopped flow reactor (analogous to a batch reactor) shows the

fluorescence. The reaction path was modeled using Kenticus™ Version 2.3 software to integrate the reaction differential equations.

Table 1. Reaction Mechanism Proposed for System with Best Estimates of Rate Constants

| Reaction # | Rate Constant | Reaction |
|---|---|---|
| R1 | 7.60E+01 | H2O2 + Fe++ ==> Fe+++ + HO + HO- |
| R2 | 3.00E+08 | HO + Fe++ ==> Fe+++ + HO- |
| R3 | 3.30E+07 | HO + H2O2 ==> H2O + HO2 |
| R4 | 1.20E+06 | HO2 + Fe++ ==> HO2- + Fe+++ |
| R6 | 5.30E+09 | HO + HO ==> H2O2 |
| R7 | 4.50E+09 | HO- + Fe+++ ==> FeOH++ |
| R9 | 4.50E+09 | HO + RH ==> H2O + Rmh1 |
| R10 | 4.50E+09 | HO + Rmh1 ==> Rmh2 |
| R11 | 4.50E+09 | HO + Rmh2 ==> Rmh3 |
| R12 | 4.50E+09 | HO + Rmh3 ==> Rmh4 |
| R13 | 4.50E+09 | HO + Rmh4 ==> Rmh5 |
| R14 | 4.50E+09 | HO + Rmh5 ==> Rmh6 |
| R16 | 4.50E+09 | Fe++ + HO- ==> FeOH+ |
| R17 | 1.35E+00 | FeOH+ ==> Fe++ + HO- |
| R18 | 5.90E+06 | FeOH+ + H2O2 ==> Fe+++ + HO + 2HO- |
| R19 | 1.20E+06 | Fe++ + HO2 ==> FeOOH++ |
| R20 | 2.70E+01 | FeOOH++ + Fe++ = FeOOHFe++++ |
| R21 | 1.80E+03 | FeOOH++ ==> Fe+++ + HO2- |
| R22 | 2.50E+04 | FeOOHFe++++ ==> Fe+++ + FeOOH+ |
| R23 | 1.00E+09 | H+ + FeOOH+ ==> Fe++ + H2O2 |
| R24 | 1.20E+06 | Fe++ + HO2 ==> Fe+++ + HO2- |
| R25 | 1.00E+07 | Fe++ + O2- ==> Fe+++ + O2-- |
| R26 | 1.50E+08 | Fe+++ + O2- ==> Fe++ + O2 |
| R27 | 9.70E+07 | HO2 + O2- ==> O2 + HO2- |
| R28 | 8.30E+05 | HO2 + HO2 ==> H2O2 + O2 |
| R29 | 7.10E+09 | HO2 + HO ==> H2O + O2 |
| R30 | 1.00E+10 | HO + O2- ==> HO- + O2 |
| R31 | 3.00E+10 | H+ + O2- ==> HO2 |
| R32 | 4.80E+05 | HO2 ==> H+ + O2- |
| R33 | 1.40E+11 | H+ + HO- ==> H2O |
| R34 | 1.80E-05 | H2O ==> H+ + HO- |
| R35 | 3.00E+10 | H+ + HO2- ==> H2O2 |
| R36 | 6.60E-02 | H2O2 = H+ + HO2- |
| R37 | 3.00E+10 | H+ + O2-- ==> HO2- |
| R38 | 1.00E-06 | HO2- = H+ + O2-- |
| R39 | 1.00E+10 | FeOH++ + HO- ==> FeOHOH+ |

Fenton's Reagent (ferrous ion and hydrogen peroxide**)** may well find widespread application in the development of mixing diagnostics. The key intermediate species in determining the rate of destruction of Rh-WT is the hydroxyl radical (OH), which reacts rapidly with a wide variety of aromatic molecules. It is therefore likely that this rate-selectable Fenton's reagent system can be used with a wide variety of fluorophores. The final products of the Fenton's Reagent/Rh-WT system are innocuous ($Fe^{+++}$, $H_2O$, $CO_2$, $O_2$), and indeed, Fenton's Reagent is often suggested for use in wastewater cleanup.

## KINETIC MECHANISM

The work of Barb, et al. (1949, 1951) provided crucial understanding of the reaction of $Fe^{++}$ with $H_2O_2$. Their work provided confirmation of the role of hydroxyl radical in the overall reaction through the initiation reaction

$$Fe^{++} + H_2O_2 \Rightarrow Fe^{+++} + OH^{\bullet} + OH^{-} \qquad (R1)$$
$$k_1 = 76\ M^{-1}\ sec^{-1}$$

Note that hydroxyl radical ($OH^{\bullet}$) and hydroxide ion ($OH^{-}$) are distinct species. The overall stoichiometry is such that one $H_2O_2$ molecule oxidizes two $Fe^{++}$ to $Fe^{+++}$.

Millero, et al.(1991) showed that an alternate, much faster path was important.

$$Fe^{++} + OH^{-} \Leftrightarrow FeOH^{+} \qquad (R16/R17)$$

$$FeOH^{+} + H_2O_2 \Rightarrow Fe^{+++} + OH^{\bullet} + 2OH^{-} \qquad (R18)$$
$$k_{18} = 5.9 \times 10^6\ M^{-1}sec^{-1}$$

Since [$FeOH^{+}$] is pH dependent, the combination of reaction (1) with reactions (2) and (3) makes the $OH^{\bullet}$ production rate pH dependent also. Early studies of the Fenton's Reagent reactions were conducted in strongly acidic solutions (typically pH = 1), presumably to simplify the system by suppressing these other reactions. A mechanism that can provide rates of destruction of Rh-WT over the pH range 1-7 must include not only these species and other minor species such as the $HO_2^{\bullet}$ radical, but also the acid-base chemistry associated with all protonated species and with $Fe^{++}$ and $Fe^{+++}$.

Table 1 lists the full reaction mechanism used in these studies. The following paragraphs describe the sources of rate constants and arguments used to estimate missing rate constants.

**R1-R14**

Reactions R1-R4 and R6 make up the essential Barb (1949, 1951) mechanism. $OH^{\bullet}$ is produced in R1, and rapidly reacts with a second $Fe^{++}$ via R2. Excessive $H_2O_2$ inhibits the conversion since R3 converts the highly reactive $OH^{\bullet}$ radical to the much more stable $HO_2^{\bullet}$ radical, which converts $Fe^{++}$ to $Fe^{+++}$ via the slower R4. $OH^{\bullet}$ radicals can recombine via R6.

R7 is not part of the essential Barb mechanism. It is included as a sink for $OH^{-}$; without R7 the calculated pH would rise to unrealistic values. However, since many of the early studies were run in strongly acidic (pH = 1) solutions, they could be modeled by fixing the pH and ignoring the $OH^{-}$ production.

Reaction R9 is the conversion of the strongly fluorescent Rhodamine WT molecule to another, non-fluorescent molecule. $k_9$, the rate constant for reaction R9, along with the [OH], determines the rate of reaction of Rhodamine WT. A literature search failed to find a measured value for $k_9$. However, examination of the extensive tables compiled by Dorfman and Adams (1973) shows that $k_9$ lies in the range (6-9) x $10^9$ $M^{-1}sec^{-1}$ for a wide range of aromatic molecules. The value used in these studies, $k_9 = 1 \times 10^{10}\ M^{-1}sec^{-1}$, was chosen before the examination of the Dorfman tables, but it is unlikely to be more that a factor of 1.5 higher than the true value. Reactions R10-R14 are included to account for the fact that Rhodamine WT has multiple hydrogens, each of which could be attacked by the highly reactive OH radical. These ill-defined product molecules were included to allow for depletion of [OH] by RH-WT. The rates for R10-R14 were taken to be the same as the rate for R9.

**R15-R39**

There is no reaction R15; it was included in order to maintain line numbering.

Reaction pairs R16/R17, R31/R32, R33/R34, R35/R36, and R37/R38 all represent acid-base chemistry for which equilibrium constants are available (estimated for R37/R38). However, no reaction rate data were found for these reactions. In these cases, the rate constant for the association reaction was estimated to be near the diffusion-limited rate, and the rate constant for the dissociation reaction was estimated. The function of these reaction pairs is to

enable the species to move toward acid-base equilibrium and yet to allow for the possibility that the reactions are actually not sufficiently fast to maintain exact equilibrium.

## APPARATUS

A schematic diagram of the apparatus is shown in Figure 3. The output beam from a Nd:YAG laser (15 pps, 532 nm, New Wave Research Gemini Dual mini-YAG) was expanded into a 20 degree fan. The measured FWHM for the (approximately Gaussian) laser sheet at its waist was approximately 400 μm; considering the distortions induced in passing through the plexiglas cells, it is probably slightly larger in these experiments. The fluorescence was imaged, perpendicular to the laser sheet, onto a SensiCam SGVA monochrome CCD camera (12 bit = 4096 counts maximum, 1280 x 1024 pixels, 9.9 μm x 9.9 μm), fitted with a Navitar Zoom 7000 lens (set at f/# 2). A glass filter (Dantec, 99C85) was used to suppress the scattered light from the laser and yet pass a major fraction of the Rh-WT fluorescence. In these experiments, the camera was electrically cooled to –40$^{o}$C, and with 2 x 2 binning, and each 2 x 2 element had a background of approximately 60 counts. The distance from the front of the laser fan optic to cell C1 was approximately 31 cm, and the distance from the cells to the camera was approximately 50 cm. Under these conditions, the width of a 2 x 2 element corresponded to a distance of 0.285 mm in the cells. The SensiCam proprietary software was used to transfer images from the camera and to save them to the hard drive of the data storage computer. In order to provide the approximately 1 ms delay time required for the camera image acquisition gate to open, the laser and the camera were triggered by separated 5V pulses from a function generator (BK Model 2001B, square wave mode).

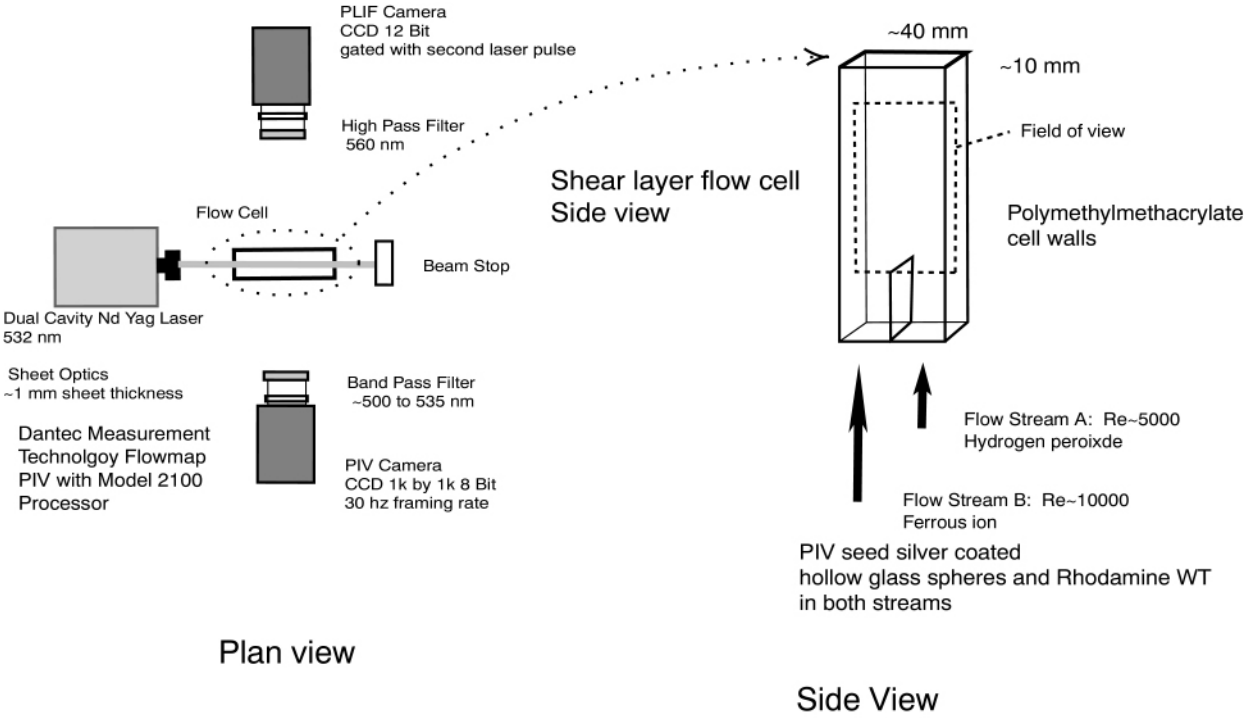


Figure 3. Optical Arrangement and Integration with Flow Cell

The flow cell, laser, optics, and cell were surrounded with a laser non-reflective adsorbing surface mounted on poster board box to reduce the amount of scattered laser light in the room. The flow cell and delivery system were designed to minimize optical distortion, produce quantifiable and controlled flow conditions, and to provide a variable shear flow with a Reynolds number (based on which cross-sectional characteristic length dimension) in the turbulence transition region (5,000-20,000). The system provided well-characterized test flows for the initial development phase and valuable information on the interrogation of more complex flows.

The flow cell is made from UV absorbing Plexiglas™ polymethylmethacrylate of 0.62 mm thickness, rectangular cross-section of 20 by 40 mm with an overall length of 22 inches with a splitter plate separating the two flows along approximately half the length of the cell. Figure 4 shows schematically the construction of the flow development section of the cell, which was mounted vertically to allow for bubbles to be expelled rapidly from the cell at the start of a run. The flow development section consists of tapered inlet transitions and flow straighteners 100 mm long with ~2 mm passages. Grids of stainless steel mesh (20 mesh) (mesh opening of 0.84 mm and wire size of 0.51 mm) were placed in each channel ~10 cm prior to the end of the splitter plate in order to eliminate large-scale flow structures and thus provide a known initial turbulence condition for the flow. The delivery system consisted of two tanks, two pumps, and two flow meters; one set for each channel. The flows were logged with a data acquisition system.

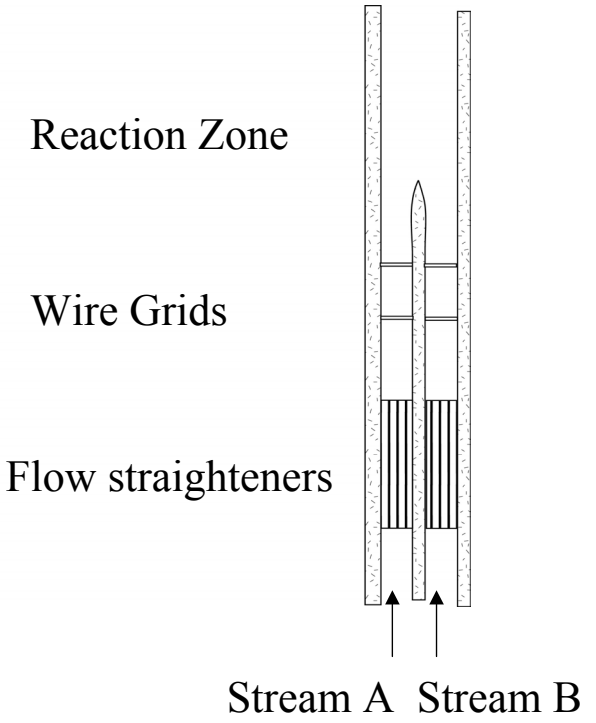


Figure 4. Schematic of Shear Cell

Figure 5 shows the linearity of the response of the measurement system. The correlation coefficient ($R^2$) is 0.99988 for values taken from a 200 by 200 pixel area with 100 images. This represents an uncertainty due to correlation of +/- 0.84% % at 95% confidence limits. The optically thin mode of operation of the fluorescent methodology is verified by the intensity profile shown in Figure 6, and is used throughout the design and analysis of the experiments. At a typical maximum (initial) fluorphore concentration, a profile of intensity shows only a 1% decrease across the cell**,** verifying optical thinness.

Based on PIV measurements the fluctuating velocity was about 2% of the mean velocity in the direction of flow. The Kolmogorov scale was estimated to be 140 micrometers based the measured turbulence intensity of 2% of the mean axial velocity, which results in a Batchelor scale of ~3 micrometers. The Batchelor scale is the scale at which the diffusion dominates mass transfer. This is contrasted with the pixel size of 500 micrometers and a thickness of the laser sheet of ~400 micrometers at half maximum. Ideally one would like to measure scalar mixing very near the Batchelor scale to fully assess the role of intermittency in turbulent mixing. Resolving to the Batchelor scale appears to be challenging, as this will lower the probe volume by a factor of $\sim 10^7$. The alternative that was chosen was to use the reactive diagnostics to assess the smallest scales of mixing.

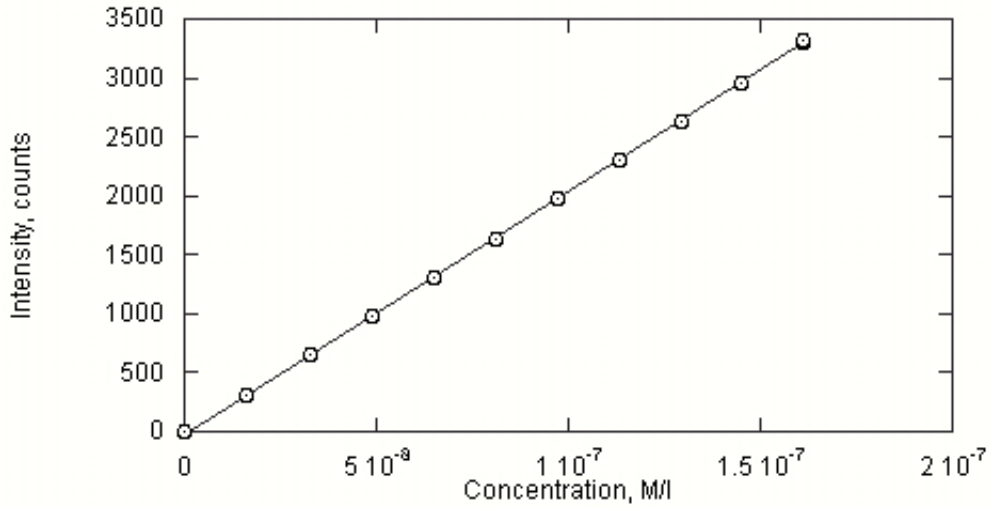


Figure 5. Calibration Response of Rhodamine WT at 532 nm Laser

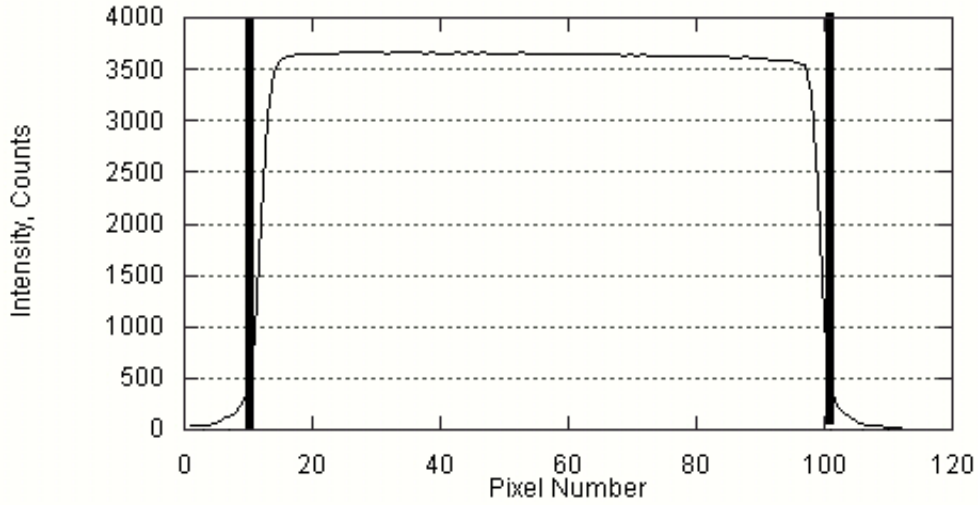


Figure 6. Intensity Profile across Cell at a $1.5 \times 10^{-7}$ M/liter Concentration of Rhodamine WT

The classic reactive diagnostics that are applicable are of two types. First the Bourne (1983, 1990) reaction classes show the formation of byproducts. This uses chemistry to produce byproducts that can be analyzed after the reaction zone to assess the small scale mixing. These systems are not spatially resolved and therefore do not lend themselves to elucidating the areas where models and physical systems differ only by an averaged resultant product distribution. As with all methods very careful control of the experimental system is required.

Acid-base reaction-based fluorescence methods have been used by many. Many of these use fluorescence that is suppressed below a pH of 11. At first view this appears to be an excellent diagnostic, as the reaction of acid and base is irreversible and has a very high reaction rate. The experimental approaches have been varied in several ways, but the issue is to avoid both the confounding of reaction and dilution and the reversibility of the fluorescence.

Analysis of reaction pathways shows the chemistry of the main pathway can be reduced to a two step method as a conceptual approximation. That is, the reaction of ferrous with hydrogen peroxide to produce the hydroxyl radical, and the reaction of the hydroxyl radical with Rhodamine WT. The reaction rate for the second reaction depends on the amount of hydroxyl radical produced by the first reaction. As the molar ratio of ferrous to Rhodamine is ca. 24,000, very large, the second reaction rate is the controlling rate inferred from experimental work and from sensitivity studies on the reaction scheme. Figure 7 is an example of a processed RPLIF image showing contours of reaction extent. The reaction extent and micromixing times are fully consistent with the reaction kinetics.

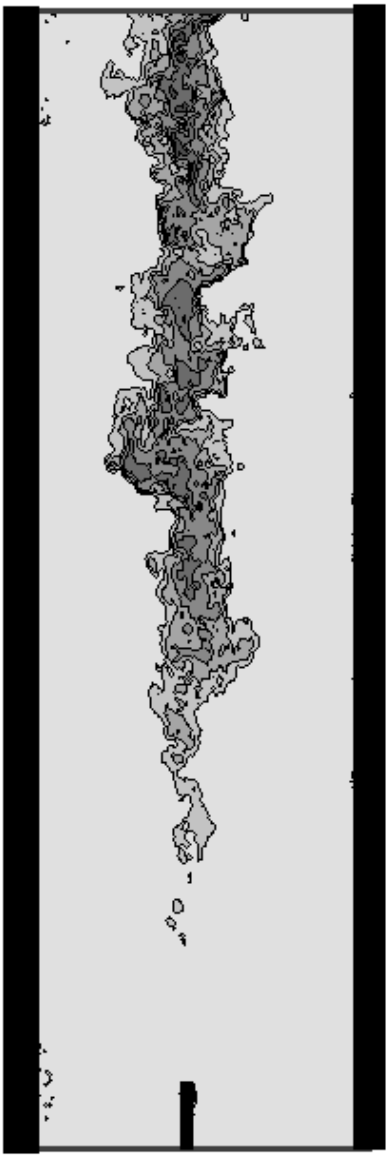

Figure 7. Instantaneous Fe(II)/$H_2O_2$ reaction zone image from flow cell. Lightest contour corresponds to 10% reaction or less; darkest, to 80% reaction.

Reactive mixing is often characterized by the Damkohler number, defined as the ratio of characteristic mixing time to characteristic reaction time. If the characteristic mixing time is the characteristic time of the Kolmogorov scale and the second is based on the reaction rate equation using the estimated reaction, the resulting Damkohler number is ca. 35. The reaction is much faster than the mixing, Da>>1. This can be adjusted by varying the concentrations of the starting reagents. However, these conditions are at a moderate Kolmogorov length scale. It would be advantageous to have a higher reaction rate.

## CHARACTERISTIC OF AN IDEAL DIAGNOSTIC

There are many perspectives to consider in developing a reactive diagnostic. Reaction kinetics must be known, and simple enough to model. Current CFD-based reaction models permit significant numbers of reactions without becoming a computational burden. Well-established kinetics is a must. Reactions that are irreversible challenge models and are relevant in solving industrial reactor design problems**.** The reaction pathways ideally would be independent of mixture fraction. Defining spatially resolved extent of reaction will enable models to be examined for regions where experiment and model show agreement and difference. Another requirement for an ideal diagnostic is that it has good fluorescence characteristics to permit spatial and temporal resolution of reaction extent. The reaction rate of the mixing-sensitive reaction must be fast relative to the mixing time. Ideally a tunable reaction rate would be most valuable.

The reagents themselves should have low to moderate cost and not have an adverse environmental impact. The cost of the fluorophore used is typically insignificant with respect to the cost of the time to conduct and analyze the experimental results. As the aqueous stream from the experiment is typically discharged after some level of pretreatment to a wastewater treatment plant it is desirable to minimize the pretreatment necessary.

## REACTIVE MIXING BENCHMARK PROPOSAL

Many reactive mixing systems have been reported in the literature. Often these are coaxial type flows. Several reported systems are pure coaxial flow – pipes within pipes or rectangular duct. Some are shear layer flows. To maximize the use of these datasets to evaluate computational models and develop new strategies to model reactive flow, a well-quantified flow field is a must. Mean flow parameters as well as turbulence parameters are required.

A proposed benchmark flow system has more richness of flow complexity and yet maintains a robustness in terms of defining the inlet conditions. Figure 8 shows the proposed concept. This is intended to provide a starting point for discussion and to highlight the need to establish a system that can be evaluated by multiple methods and researchers.

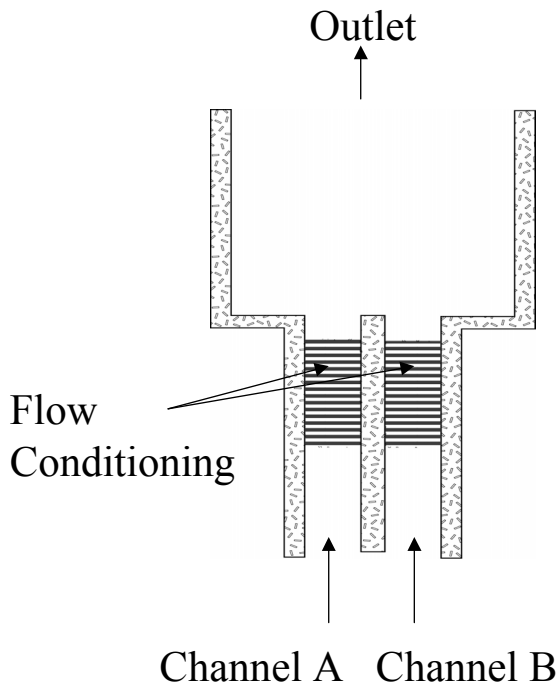


Figure 8. Proposed Benchmark Reacting Flow Geometry

There are other potential benchmark flows that may be considered, including unequal flows such as "T" mixers. In part the choice of a backward facing step is advantageous, because the literature is replete with studies of the fluid dynamics phenomenology.

**REFERENCES**

Barb, W. G., J. H. Baxendale, P. George, and K.R. Hargrave (1949). "Reactions of Ferrous and Ferric Ions with Hydrogen Peroxide", Nature **163**, pp. 692-4

Barb, W. G., J. H. Baxendale, P. George, and K.R. Hargrave (1951). "Reactions of Ferrous and Ferric Ions with Hydrogen Peroxide. Part II – The Ferric Ion Reaction", Trans. Faraday Soc. **47**, pp. 591-616

Boedec, T. and S. Simoens (2001). "Instantaneous and Simultaneous Planar Velocity Measurements of Two Phase for Turbulent Mixing of High Pressure Sprays", Exp. Fuids **31**, pp. 506-518

Bourne, J. R., U. Moergeli, and P. Ryes (1977). Mixing and Fast Chemical Reaction: Influence of Viscosity on Product distirbuiton, 2 Europ. Conf. Mixing, BHRA, Cranfield, pp. 41-45

Bourne, J.R., O. M. Kut, J. Lenzner and H. Marier (1990). **"**Kinetics of the diazo coupling between 1-napthol and diazotized sulfanilic acid", Ind Engr Chem Res **29**, pp. 1761-1765

Catrakis, H. J. and P. E. Dimotakis (1996). "Scale distributions and fractal dimensions in turbulence," Physical Review Letters **77**, p. 3795

Catrakis, H. J. and P. E. Dimotakis (1996a). "Mixing in turbulent jets: scalar measures and isosurface geometry," J. Fluid Mech. **317**, p. 369

Coleman, H. and Steele, W.G. (1989). *Experimental and Uncertainty Analysis for Engineers*, John Wiley & Sons, NYC.

Dahm, W. J. A. and P. E. Dimotakis (1990). "Mixing at large Schmidt number in the self-similar far field of turbulent jets," J. Fluid Mech. **217**, p. 299

Dahm, W. J. A. and P. E. Dimotakis (1990a). "Measurements of entrainment and mixing in turbulent jets," AIAA Journal **25**, p. 1216

Dimotakis, P. E., R. C. Miake-Lye, and D. A. Papantoniou (1983). "Structure and dynamics of round turbulent jets," Phys. Fluids **26**, p. 3185

Distelhoff, M. F. W., A. J. Marquis, J. M. Nouri, and J. H. Whitelaw (1997). "Scalar mixing measurements in batch operated stirred tanks," Can. J. Chem. Eng. **75**, p. 641

Dorfman, L. M. and G. E. Adams (1973). "Reactivity of the Hydroxyl Radical in Aqueous Solutions", Report No. NSRDS-NBS-46, U.S. Government Printing Office, Washington, D.C.

Hasselbrink, E. F., D. Han, M. G. Mungal, and R. K. Hanson (1998). "Simultaneous PIV and PLIF Measurements in Nonpremixed Transverse Jet Flames", 9th Int. Symp. Appl. Laser Tech. Fluid Mech., Lisbon

Houcine, I., B. Marcant, H. Vivier, E. Plasari, R. David, and J. Villermaux (1994). "Comparison of mixing action of several stirrers by laser sheet visualization and image processing," ICHEME Symposium Series **136**, p. 97

Houcine, I., H. Vivier, E. Plasari, R. David, and J. Villermaux (1996). "Planar laser induced fluorescence technique for measurements of concentration fields in continuous stirred tank reactors," Experiments in Fluids **22**, p. 95

Karasso, P. S. and M. G. Mungal (1997). "PLIF measurements in aqueous flows using the Nd:YAG laser", Experiments in Fluids **23**, pp. 382-387

Kintecus, Version 2.3 (2001). James C. Ianni, jamesianni@nestscape.com

Koochesfahani, M. M. and P. E. Dimotakis (1986). “Mixing and chemical reactions in a turbulent liquid mixing layer,” J. Fluid Mech. **170**, p. 83

Komori, S. K, K. Nagata, T. Kanzaki, and Y. Murakami (1993). “Measurements of Mass Flux in a Turbulent Liquid Flow with Chemical Reaction”, AIChE J. **39** (10), pp. 1611-1620

Milero, F., S. Sotolongo, D. Stade. and C. Vega (1991). “Effect of Ionic Interactions on the Oxidation of Iron(II) with Hydrogen Peroxide in Aqueous Solutions”, J. Solution Chem. **20**, pp. 1079-92

Miller, P. L. and P. E. Dimotakis (1996). “Measurements of scalar power spectra in high Schmidt number turbulent jets,” J. Fluid Mech. **308**, p. 129

Sen, S., K. Tsai, P. Gillis, R. Larkins, R. Spradling, and L. A. Melton (1999). “Evaluation of Micro-mixing Models in Simulating Liquid Phase Turbulent Reacting Flow”, AIChE Annual Meeting, Dallas, TX, Oct. 31-Nov.5, 1999, Paper 309i.

Turner Designs, www.turnerdesigns.com; accessed December 28, 2001.

Vivier, H., I. Houcine, E. Plasari, R.David, and J. Villermaux (1994). “Application of a planar laser induced fluorescence technique to characterize mixing in a pilot scale stirred tank,” Proc. 4th Int. Conf. Fluid Contol, Fluid measurement and Visualization, Tolouse, **4**, p. 1107

Wang, G. R. and H.E. Fiedler (2000). "On high resolution scalar measurement with LIF, Part 1: Photobleaching and Thermal blooming", Exp. in Fluids **29**, pp. 257-264

Wang, G. R. and H.E. Fiedler (2000). "On high resolution scalar measurement with LIF, Part 2: The noise characteristic", Exp. in Fluids **29**, pp. 265-267